Supplement of Atmos. Chem. Phys., 25, 3603–3621, 2025
https://doi.org/10.5194/acp-25-3603-2025-supplement

Atmospheric Chemistry and Physics
Open Access
EGU

Supplement of

Effects of 2010–2045 climate change on ozone levels in China under a carbon neutrality scenario: key meteorological parameters and processes

Ling Kang et al.

Correspondence to: Hong Liao (hongliao@nuist.edu.cn)

S1. Formaldehyde nitrogen ratio (FNR)

For discussion of ozone (O_3) sensitivity to its precursors, the formaldehyde nitrogen ratio (FNR) (Jin and Holloway, 2015) is used to feature the O_3 formation regime, with FNR<1.0 representing VOC-limited regimes, FNR> 2.0 representing NO_x-limited regime, and FNR between 1.0 and 2.0 representing transitional regime. For model evaluation, monthly mean Aqua OMI tropospheric columns of nitrogen dioxide (NO_2) (Boersma et al., 2018) and formaldehyde (HCHO) (De Smedt et al., 2015) products in 2015 are obtained from https://www.temis.nl/airpollution/, with resolutions of 0.125° × 0.125° and 0.25° × 0.25°, respectively. The satellite observations are interpolated into 2° × 2.5° resolution to be consistent with that of model outputs. Figure S7 evaluates the simulated present-day tropospheric columns of NO_2 and HCHO in CpdEpd simulation by comparing with Aqua OMI satellite observations. The tropospheric columns of NO_2 and HCHO levels are overestimated by 4.4 and 1.1 10^{15} molec cm^{-2} in EC and by 1.8 and 0.7 10^{15} molec cm^{-2} nationwide, respectively. We also compared the simulated surface NO_2 concentrations with observations from CNEMC in Fig. S8. The model generally captured the observed monthly variation in surface NO_2 concentrations in EC, NCP, and YRD, with R values of 0.44-0.70. The systematic low biases of surface NO_2 concentrations in the GEOS-Chem model (NMBs ranging from -51.7% to -19.2% in this work) were also reported in previous studies (Qu et al., 2020; Qu et al., 2022; Fang et al., 2024), because of the lack of representation of the spatial gradients in NO_2 observations within the coarse GEOS-Chem grid cells (Qu et al., 2022).

Table S1. Information of climate models in CMIP6 used in this study.

Model	N	Member_id (Historical/SSP1-1.9)
CanESM5	2	r1i1p1f1, r1i1p2f1
GFDL-ESM4	1	r1i1p1f1
GISS-E2-1-G[a]	3	r1i1p1f2, r1i1p3f1, r1i1p5f1
GISS-E2-1-H[b]	2	r1i1p1f2, r1i1p3f1
MIROC-ES2H	1	r1i1p4f2
MIROC-ES2L	1	r1i1p1f2
Total	10	

[a, b] GISS-E2.1-G and GISS-E2.1-H are coupled models of the GISS-E2.1 atmospheric model with the GISS and HYCOM ocean models, respectively.

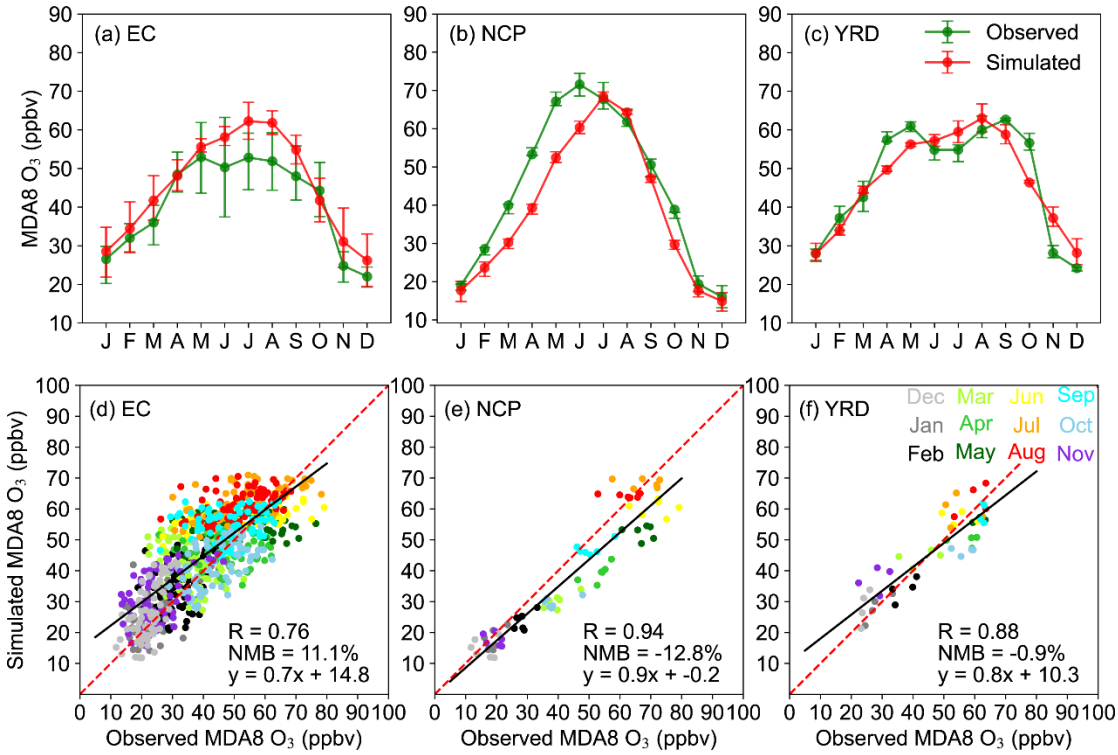

Figure S1. (a)-(c) Monthly variations in simulated and observed MDA8 O_3 concentrations (ppbv) over (a) EC (with a total of 68 grids), (b) NCP (with a total of 6 grids), and (c) YRD (with a total of 4 grids) regions. Bars represent the range from first to third quartiles of all grid samples in this region. (d)-(f) The scatterplot of simulated versus observed monthly mean MDA8 O_3 concentrations for grids in EC, NCP, and YRD. The linear fit (black solid line and equation), correlation coefficient (R), and normalized mean biases (NMB) that calculated for grids in these three regions are also shown when all of the year 2015 data are considered.

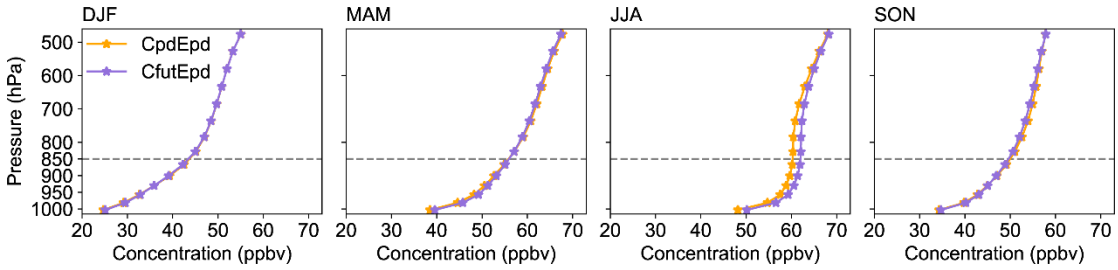

Figure S2. Vertical profile of seasonal mean O_3 concentrations (ppbv) over EC in CpdEpd and CfutEpd simulations.

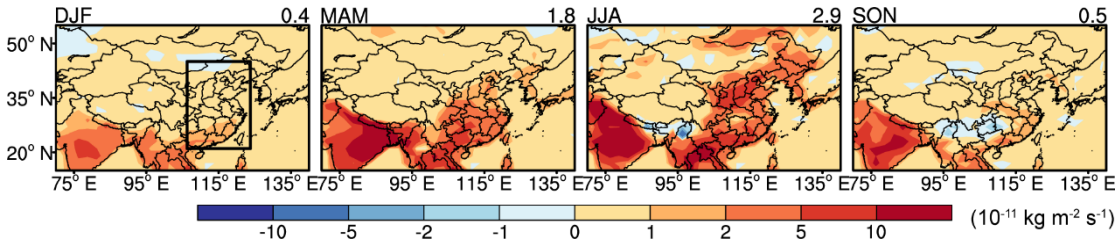

Figure S3. Seasonal mean changes in biogenic emission rates of VOCs (10^{-11} kg m^{-2} s^{-1}) due to climate change over 2010-2045. The black rectangle indicates the domain of EC, and the top right number of each panel is the regional mean value for EC.

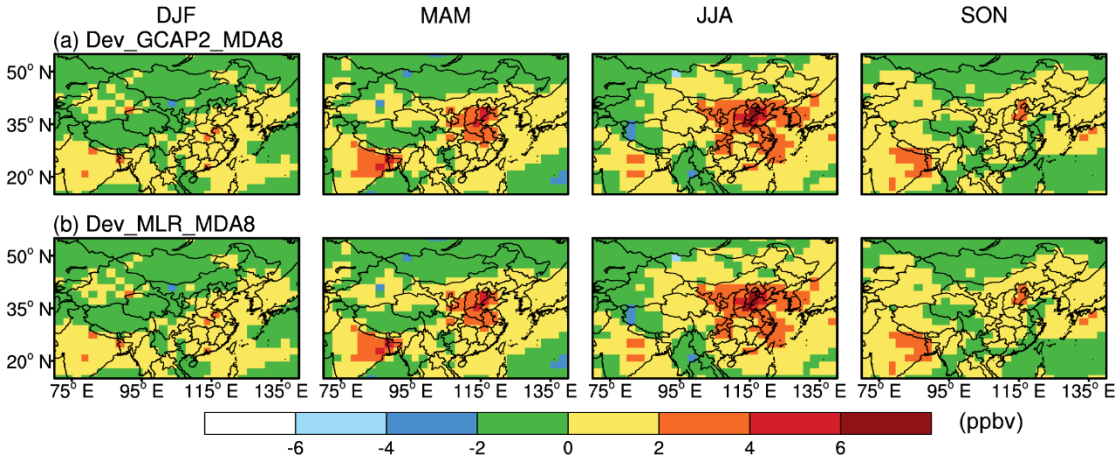

Figure S4. Comparisons of the spatial distributions of climate-induced seasonal mean MDA8 O_3 changes simulated by (a) GCAP 2.0 (Dev_GCAP2_MDA8) with those predicted by (b) stepwise MLR model (Dev_MLR_MDA8).

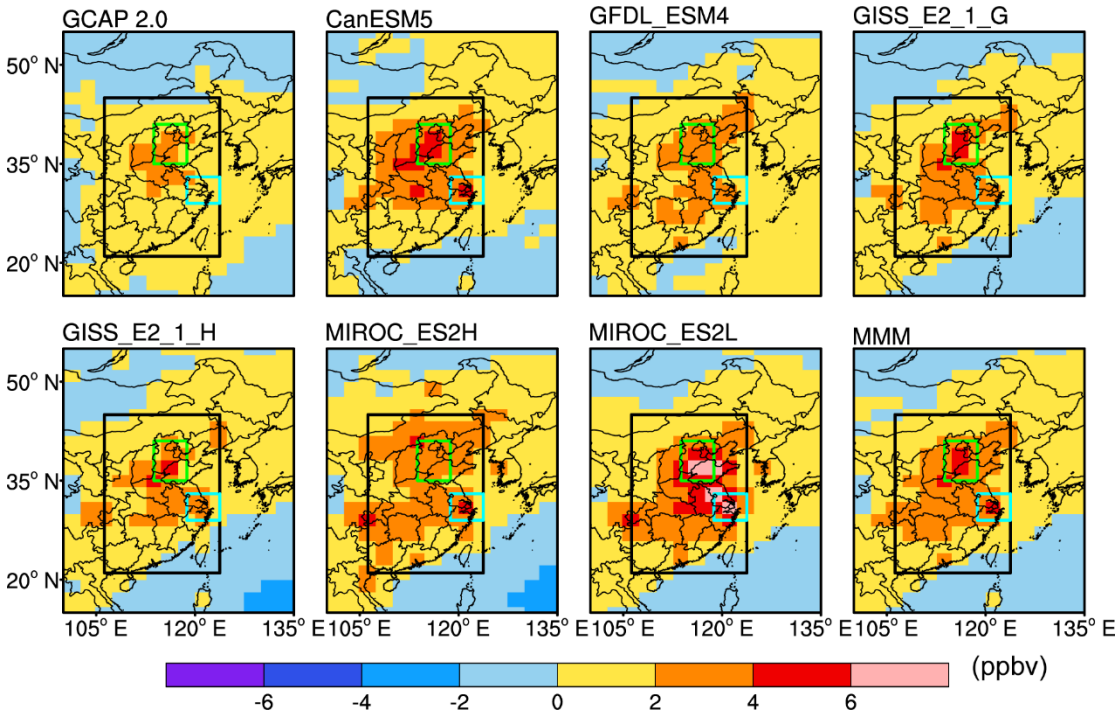

Figure S5. The spatial distributions of climate-driven changes in annual mean MDA8 O_3 concentrations (ppbv) in EC projected by MLR model using the climate outputs from GCAP 2.0 and the other six CMIP6 models under SSP1-1.9 scenario. The multi-model mean (MMM) is calculated from the average of the six CMIP6 models.

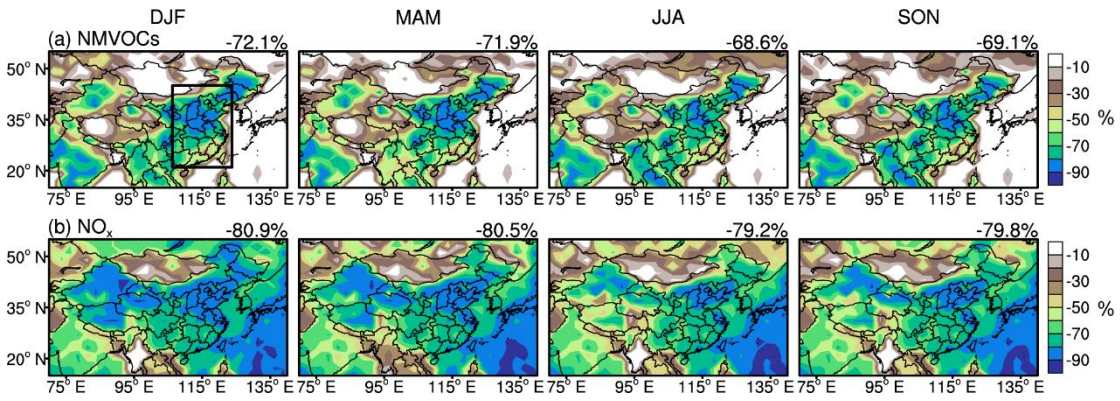

Figure S6. Percentage changes (%) in anthropogenic emission rates of (a) NMVOCs and (b) NO_x in 2050 relative to 2015 under SSP1-1.9 scenario. The black rectangle indicates the domain of EC, and the top right number of each panel is the regional mean value for EC.

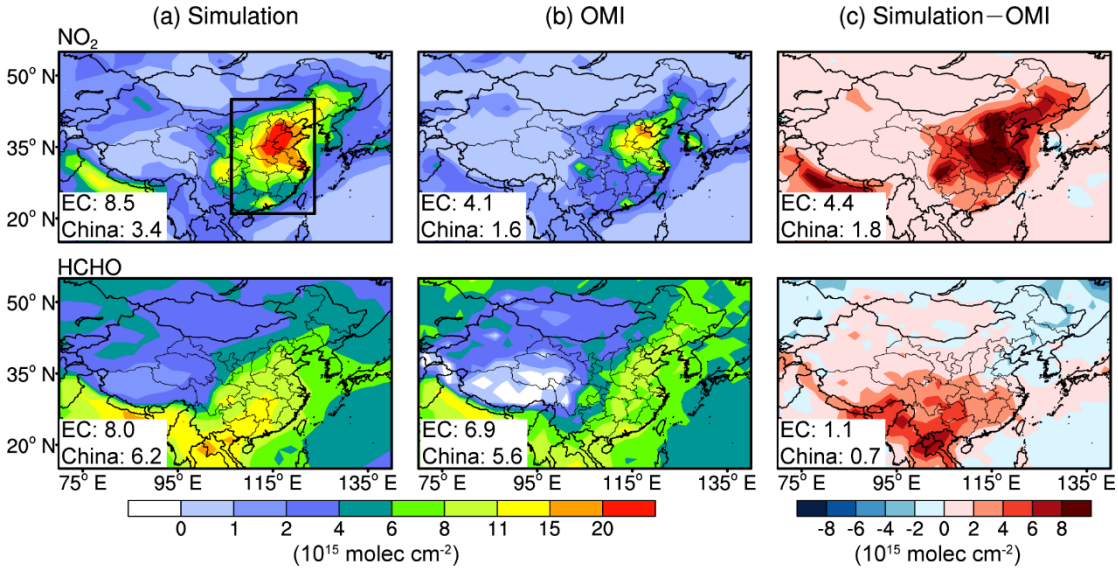

Figure S7. (a) Simulated and (b) OMI retrieved annual mean tropospheric columns of nitrogen dioxide (NO_2) and formaldehyde (HCHO) (10^{15} molec cm^{-2}) in 2015 in China, and (c) their difference. The black rectangle indicates the domain of EC, and the regional mean values for EC and the whole country are shown in the bottom left corner of each panel.

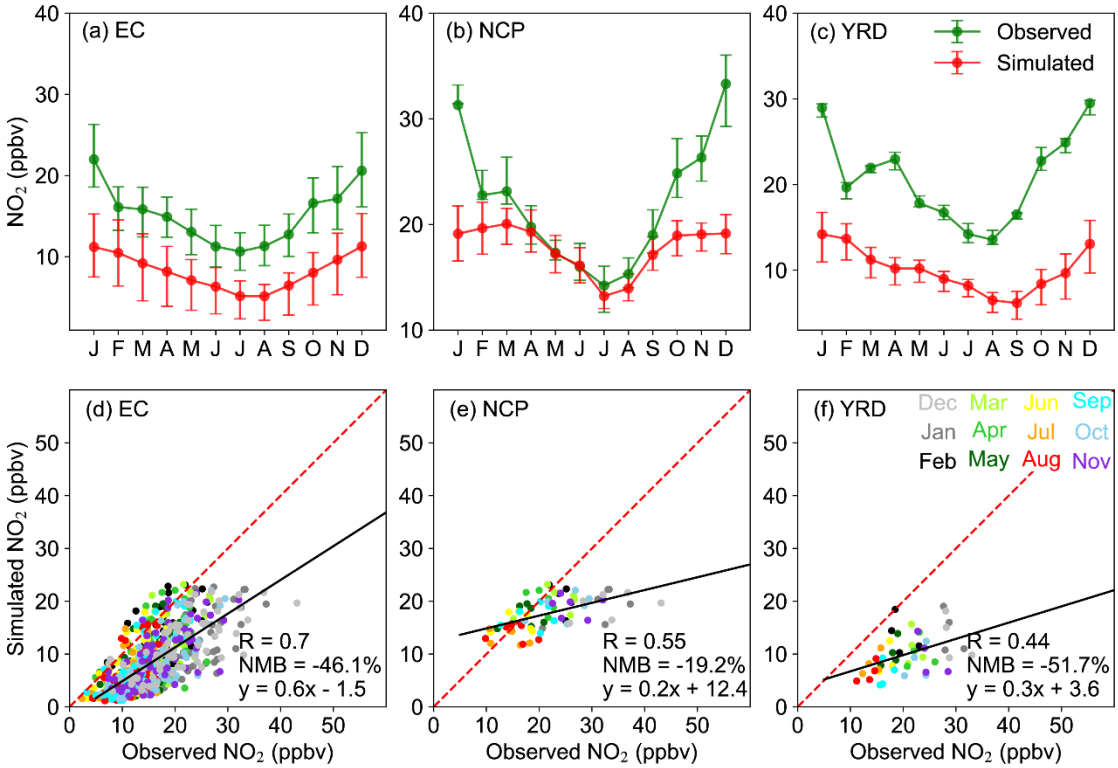

Figure S8. (a)-(c) Monthly variations in simulated and observed surface NO_2 concentrations (ppbv) over (a) EC (with a total of 68 grids), (b) NCP (with a total of 6 grids), and (c) YRD (with a total of 4 grids) regions. Bars represent the range from first to third quartiles of all grid samples in this region. (d)-(f) The scatterplot of simulated versus observed monthly mean surface NO_2 concentrations for grids in EC, NCP, and YRD. The linear fit (black solid line and equation), correlation coefficient (R), and normalized mean biases (NMB) that calculated for grids in these three regions are also shown when all of the year 2015 data are considered.

References

Boersma, K. F., Eskes, H. J., Richter, A., De Smedt, I., Lorente, A., Beirle, S., van Geffen, J. H. G. M., Zara, M., Peters, E., Van Roozendael, M., Wagner, T., Maasakkers, J. D., van der A, R. J., Nightingale, J., De Rudder, A., Irie, H., Pinardi, G., Lambert, J.-C., and Compernolle, S. C.: Improving algorithms and uncertainty estimates for satellite NO_2 retrievals: results from the quality assurance for the essential climate variables (QA4ECV) project, Atmos. Meas. Tech., 11, 6651-6678, https://doi.org/10.5194/amt-11-6651-2018, 2018.

De Smedt, I., Stavrakou, T., Hendrick, F., Danckaert, T., Vlemmix, T., Pinardi, G., Theys, N., Lerot, C., Gielen, C., Vigouroux, C., Hermans, C., Fayt, C., Veefkind, P., Müller, J. F., and Van Roozendael, M.: Diurnal, seasonal and long-term variations of global formaldehyde columns inferred from combined

OMI and GOME-2 observations, Atmos. Chem. Phys., 15, 12519-12545, https://doi.org/10.5194/acp-15-12519-2015, 2015.

Fang, L., Jin, J., Segers, A., Li, K., Xia, J., Han, W., Li, B., Lin, H. X., Zhu, L., Liu, S., and Liao, H.: Observational operator for fair model evaluation with ground NO_2 measurements, Geosci. Model Dev., 17, 8267-8282, https://doi.org/10.5194/gmd-17-8267-2024, 2024.

Jin, X. and Holloway, T.: Spatial and temporal variability of ozone sensitivity over China observed from the Ozone Monitoring Instrument, J. Geophys. Res.: Atmos., 120, 7229-7246, https://doi.org/10.1002/2015jd023250, 2015.

Qu, Z., Henze, D. K., Cooper, O. R., and Neu, J. L.: Impacts of global NO_x inversions on NO_2 and ozone simulations, Atmos. Chem. Phys., 20, 13109-13130, https://doi.org/10.5194/acp-20-13109-2020, 2020.

Qu, Z., Henze, D. K., Worden, H. M., Jiang, Z., Gaubert, B., Theys, N., and Wang, W.: Sector-Based Top-Down Estimates of NO_x, SO_2, and CO Emissions in East Asia, Geophys. Res. Lett., 49, https://doi.org/10.1029/2021gl096009, 2022.